Influence of Fine Structure on the Torsional Fatigue Behavior of Poly(ethylene Terephthalate) Fibers

LU FU-MIN,* B. C. GOSWAMI,† J. E. SPRUIELL,‡ and K. E. DUCKETT,§ *Textiles, Merchandising, and Design, The University of Tennessee, Knoxville, Tennessee 37996*

Synopsis

Three experimental poly(ethylene terephthalate) fibers have been spun and then drawn at three different temperatures (70°C, 90°C, and 110°C) in such a way that the drawn fibers possess different orientations and crystallinities but retain the same diameters. Wide angle X-ray diffraction and birefringence measurements have been used to characterize orientation and crystallinities of the fibers. The influence of fine structure on the torsional fatigue behavior of the melt spun and drawn PET fibers has been studied by subjecting them to 1.7 Hz torsional cyclic deformation at various amplitudes. Fracture morphology was found to be strongly influenced by the degree of orientation and crystallinity. Highly oriented and crystalline structures tended to separate into a highly fibrillated structure. Fibers of low draw ratio exhibited initial deterioration of the surface structure with the generation of transverse cracks (perpendicular to the fiber axis). Subsequent torsional loading of the structure generated an increase in longitudinal cracks which finally resulted in the catastrophic failure of the fiber. The extent of fibrillation was found to be a function of draw ratio (orientation) and crystallinity. The amplitude of torsional strain was also found to have an effect on the intensity of fibrillation and the number of cycles to fiber failure.

INTRODUCTION

Fatigue properties and fracture morphology of polymeric fibers have been classical subjects of research of the past few decades.[1] To date, much of the published literature in this area[2-7] has been concerned with the fatigue loading conditions that involve cyclic tension or tension–compression modes of deformation. Van der Vegt[8] began an investigation on the torsional fatigue of fibers through the comparison of the fatigue behavior of different types of fibers. The results of torsional fatigue properties of polyester fibers[9] have been more recently reported, but these did not deal decisively with the effect of initial fiber structure on the torsional fatigue characterization or on deterioration of mechanical properties by the fatigue process. These effects are clearly of great significance to textile designers because the life of many textile structures will be fatigue-limited. Moreover, the mechanism of the torsional fatigue process and its contribution to fracture morphological alteration are of great interest but are still incompletely understood and warrant further analysis. The apparatus designed by Duckett and

* On leave from The Institute of Beijing Chemical Fiber, Beijing, China.
† Present address: Clemson University, Clemson, SC 29631.
‡ Polymer Engineering.
§ Agricultural Engineering.

Journal of Applied Polymer Science, Vol. 30, 1859–1874 (1985)

CCC 0021-8995/85/051859-16$04.00

Goswami[10] for cyclicly fatiguing fibers has been used in this study to accumulate a range of torsional levels for more clearly interpreting the structural deterioration of single PET fibers. Tensile strength, as a stochastic variable of the level of fatigue, has also been studied. The multistation capability of the instrument has provided the replications necessary to establish correlation between stochastic variables and material parameters.

Because of the great depth of focus, scanning electron microscopy (SEM) was used to detect crack initiation on fibers and examine the fiber fracture morphologies.[11] Numerous specimens, having different internal structures and fatigued to different levels, were examined using SEM. This clarified the process of deterioration of fiber structure from torsional fatigue and its contribution to the reduction of tensile breaking levels.

EXPERIMENTAL

Fatigue Testing Procedure

The fatigue apparatus has recently been described in some detail,[10] although a few minor changes have been made to more efficiently prepare and mount specimens. Basically the apparatus consists of six machinist's dial indicators whose center shafts cyclically twist single fibers attached to the ends of the shafts. In practice, a short length of fiber is attached to two pieces of brass strip acting as sample clamps. One brass bar is attached to the rotary shaft of the dial indicator above; the other is free to move up and down on a track as necessary, but not free to rotate. The weight of the lower bar provides a constant tension on the fiber during the twist cycle. The length of the fiber can be set during mounting to provide the desired torsional strain amplitude. The time to failure is monitored electronically by a timer system when the lower bar, due to the failure of a fiber, drops and disconnects the circuit of a clocking system. The total number of turns of the rotary shaft is eighteen. When the fiber is mounted with rotary shaft at the center of its range, the twist to the fiber is ± 9.

The torsional strain α at the surface of fibers with circular cross section was calculated from

$$\tan \alpha = \frac{\pi D n}{h}$$

where D is the fiber diameter, n the number of revolutions (9 in this case), and h the fiber gauge length. Essentially, α is the helix angle defined as the angle between a longitudinal line drawn on the fiber surface at zero twist and its orientation following the twist.[9] The level of torsional strain can be varied by changing the gauge length of the fiber. The apparatus offered the capability of subjecting fibers to a rather wide range of amplitudes of cyclic torsional deformation (i.e., from 3° to 40°) while under a tensile load of 0.42 g, the weight of the lower bar. Specimen lengths were varied from 2 mm to 1.5 cm to obtain the aforementioned range of strain amplitudes. All tests were carried out at a frequency of 8 Hz.

TABLE I
Spinning and Fiber Properties

	Draw ratio		
	1.65	3.64	5.08
Fiber diameter (μm)	47.0	49.0	51.0
Density (g/cc)	1.3422	1.3742	1.3822
Crystallinity (%) by density	6	35	42
Crystallinity (%) by X-ray	10	28	33
Birefringence	0.030	0.169	0.217
Herman's orientation function			
f_c	0.40	0.92	0.95
f_{am}	0.08	0.60	0.82
f_{avg}	0.11	0.69	0.86
Initial modulus E (GPa)	0.20	0.85	1.22
Tenacity T_e (GPa)	0.22	0.36	0.57
Elongation (%)	157	57	20

Samples which had been subjected to torsional test for a preset period of time were carefully removed from the six stations of the instrumentation and divided into two groups. One group was used to examine the surface morphology using both optical and scanning electron microscopy (SEM). The other group was used to measure the residual tensile strength in an Instron tensile testing machine. The fibers mounted on the brass strips were directly transferred to the clamps of the Instron machine. For tensile tests load cell "B" with a 100-g full scale load was used. The fracture morphology of tensile break samples following fatigue tests was observed and interpreted from SEM observations.

Sample Preparation and Characterization

The samples studied in the present research were monofilament PET fibers spun and drawn in our laboratories. The PET bright pellets used in this work were supplied by the Eastman Company.

These materials were processed to obtain a wide range of molecular orientations and crystallinities. For the sake of reducing the influence of sample geometry, it was desirable to use fibers having approximately the same diameter but differing internal structure. To achieve this, a series of as-spun fibers of different diameters were extruded at spinning temperatures of 295°C. Subsequently, these fibers were drawn to different draw ratios at 90°C. The draw ratios of the final samples were 5.08, 3.64, and 1.65 with diameters of 50, 49, and 47 μm, respectively (Table I).

Fiber structural properties were determined using several techniques. The birefringence of the drawn fibers was measured using a Leitz polarizing microscope with Berek compensator. The X-ray diffraction method of Farrow[12,13] was used to determine crystallinity and crystalline orientation. The Herman's crystalline orientation function f_c is given by

$$f_c = 1 - \frac{3}{2}(\overline{\cos^2 \phi}_{a,z} + \overline{\cos^2 \phi}_{b,z})$$

where $\phi_{a,z}$ and $\phi_{b,z}$ are angles between the normals to the (100) and (010) crystalline planes, respectively, and the fiber axis. Amorphous orientation was obtained from the relation

$$f_{am} = \frac{\Delta - Xf_c\Delta_{cr}^0}{(1 - X)\Delta_{am}^0}$$

where Δ is the measured birefringence of the fiber, X is the fraction of the cystallinity of the fiber calculated from X-ray data, Δ_{cr}^0 and Δ_{am}^0 are the intrinsic birefringences of crystalline and amorphous PET, respectively,[14] and f_c and f_{am} are crystalline and amorphous orientation functions.

The densities of drawn fibers were measured using a density gradient column, and the mechanical properties were determined using an Instron tensile testing machine stationed in a conditioned room at 20°C and 65% RH. A summary of the physical parameters is presented in Table I.

RESULTS AND DISCUSSION

General Phenomena of Mechanical Degradation

When a fiber is subjected to a fixed cyclic torsional strain, three general stages of the fatigue process may be expected. During the first few hundred cycles at a twist amplitude of 15°, the homogeneous macroscopic appearance of the material is maintained. At this stage, however, molecular chains near the surface of the fiber are stretched and some of the weaker van der Waal's bonds are broken.[11] For low draw ratios where the amorphous content is large, local molecular rearrangements are accompanied by an increase in free volume and generation of microvoids.[§] At high draw ratios, on the other hand, the ends of microfilbrils preferentially situated on the outer surface of the fiber retract under stress[15] and decrease the orientation of the chains. The tensile strength drops, and some microcracks are formed. These microvoids then act as stress concentrators and play an important role in initiating cracks toward the interior of the fiber.

The onset of the propagation of cracks is associated with the formation of cloudy spots appearing at points on the surface of the fiber. The origin of the phenomenon is presumably due to the coalescence of macrovoids which can be seen under the optical microscope. For low draw ratio fibers, intensive whitening spots are observed, presumably as voids are created from crack propagation. For highly drawn fibers, the initial white spots are widely spread along the direction of crack propagation on the fiber surface during the fatigue process. Finally, the coalescence of such cracks subsequently gives rise to the fibrillar fracture. The breakage of some of the microfibrils is rapidly manifested in severe deterioration of mechanical properties of the fiber.

[§] The use of terms microvoids, voids, or microcracks is made to describe the process that is going on inside the structure at the molecular level and is only speculative, while macrovoids and cracks signify the observed features in the structure.

Effect of Draw Ratio and Strain Amplitude on Torsional Fatigue

One of the important aspects of the behavior of fibers subjected to torsional fatigue cycling is the gradual breakdown of the structure. To ascertain the extent of deterioration, the residual tensile strengths of individual filaments of various draw ratios were measured with the Instron on fibers whose torsional strain amplitudes were fixed at 15° under tensile loads of 0.169 mN/den.

There was no recognizable strength loss during the first 1000 cycles in fibers of 1.65 draw ratio (DR). Beyond that point, however, the reduction in relative strength was abrupt, losing 70% of its initial strength within 500 additional torsional cycles as shown in Figure 1(a). This figure also shows the typical stress–strain relationships of the original and fatigued samples. Strength of the low draw ratio fiber continued to decrease rapidly with torsional fatigue, until catastrophic failure of the fiber structure occurred at around 25,000 cycles. Thus, the fiber structure retained its initial integrity in the early stages of fatigue cycling, after which the structure rapidly broke down. The sequence of morphological changes began with transverse cracking, thereafter forming longitudinal cracks which eventually produced a ropelike structure at specific locations along the filament length as shown in Figures 2(a)–(d).

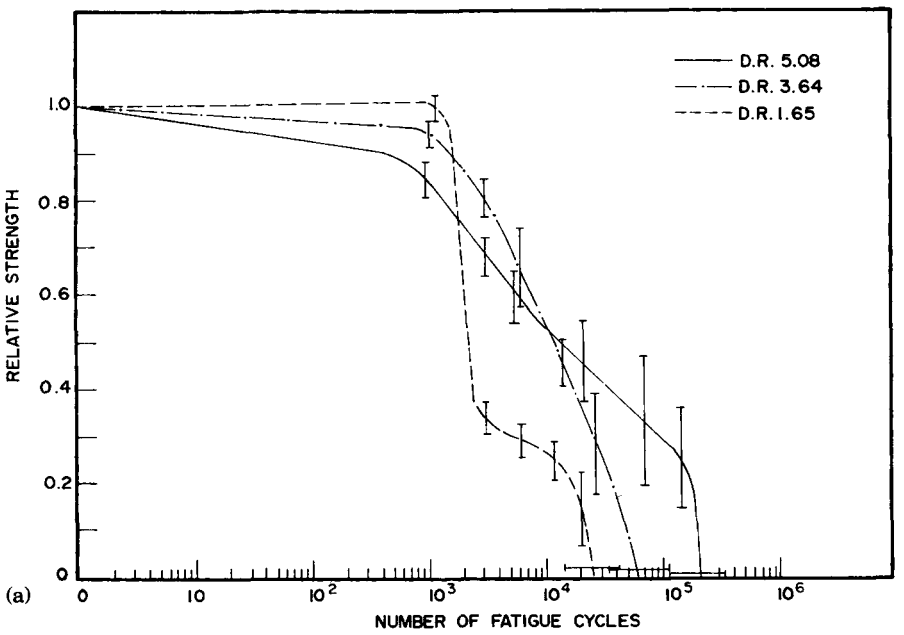

Fig. 1. Relationship between torsional fatigue cycles and strength of poly(ethylene terephthalate) fibers: (a) Fatigue cycles vs. relative strength, strain amplitude 15°: (—) DR 5.08; (— · —) DR 3.64; (- - -) DR 1.65. (b) Stress–strain curves of original drawn fibers: (X) DR 5.08; (○) DR 3.64; (□) DR 1.65. (c) Stress–strain curves of 1.65 DR fatigued fibers: (●) control; (○) 1000 cycles; (□) 6000 cycles; (d) Stress–strain curves of 3.64 DR fatigued fibers: (●) control; (X) 1000 cycles; (○) 6000 cycles; (□) 27,000 cycles. (e) Stress–strain curves of 5.08 DR fatigued fibers: (●) control; (□) 1000 cycles; (X) 6000 cycles; (○) 69,000 cycles. (f) Stress–strain curves of 1.65 (●), 3.64 (□), and 5.08 (○) DR after 6000 fatigue cycles.

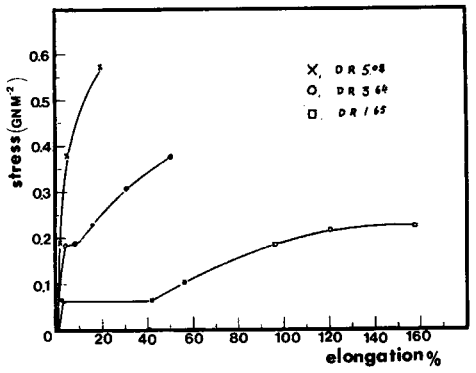

(b)

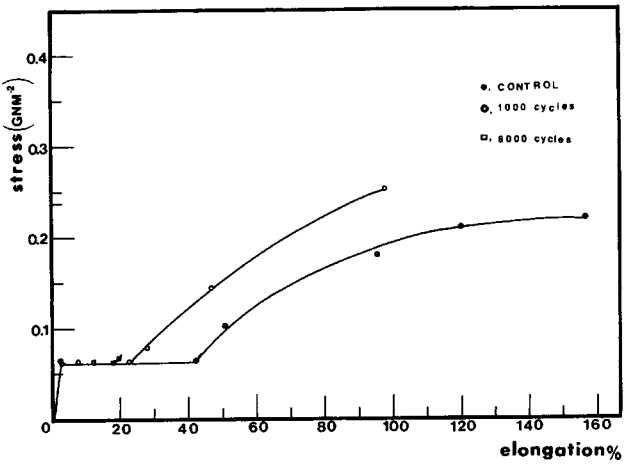

(c)

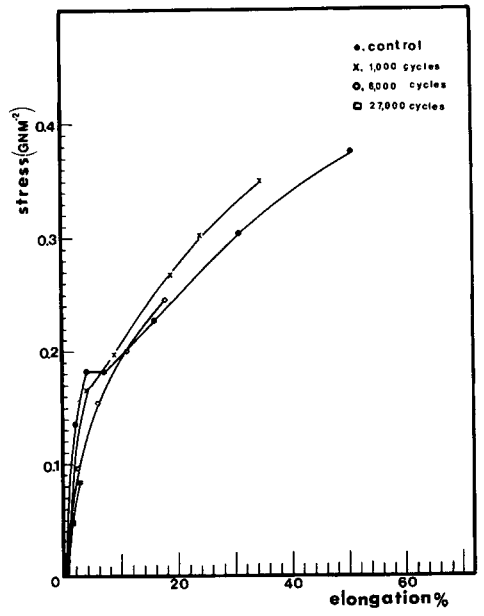

(d)

Fig. 1. *(Continued from the previous page.)*

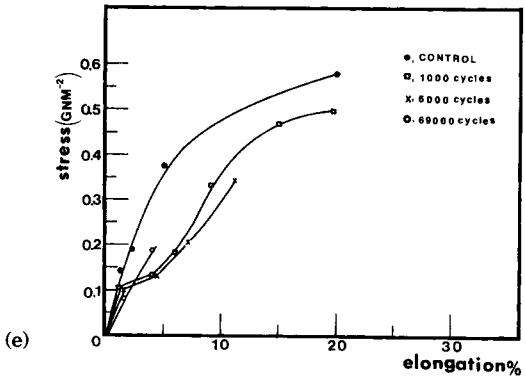

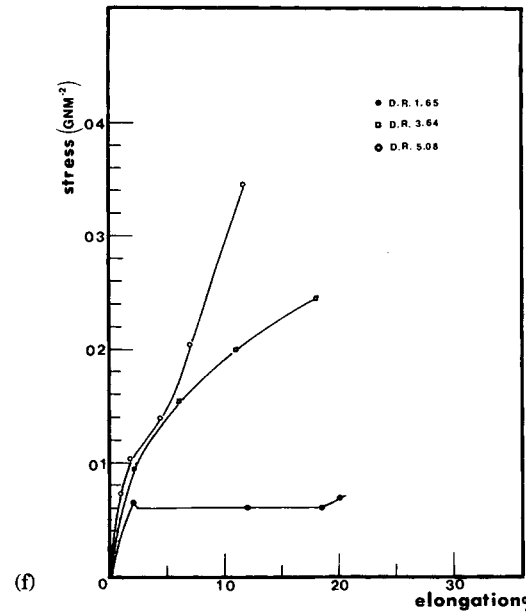

Fig. 1. *(Continued from the previous page.)*

There is a very slight loss in strength in the early stages of fatigue of fibers with 3.64 DR. Relative strength decreases approximately 5% during the first 1000 cycles. Thereafter, strength losses uniformly increase with the number of torsional oscillations. Fatigue failure is generally reached at less than 100,000 cycles. Surface morphology is distinctly different from that observed on 1.65 DR fibers. The initial transverse cracking seems to be absent [Figs. 3(a)–(c)]. The appearance of longitudinal cracking is easily identified in SEM micrographs after a few thousand torsional oscillations, and they increase in number with continued levels of fatigue. This type of behavior has very important implications in the gradual attrition of the structure as will be discussed later. The number of cracks observed is less in the case of low draw ratio, and the size of fibrillar bundles becomes smaller with increasing draw ratio. The tensile strength of the 5.08 DR samples are lowered to about 90% of the initial values after 1000 cycles of

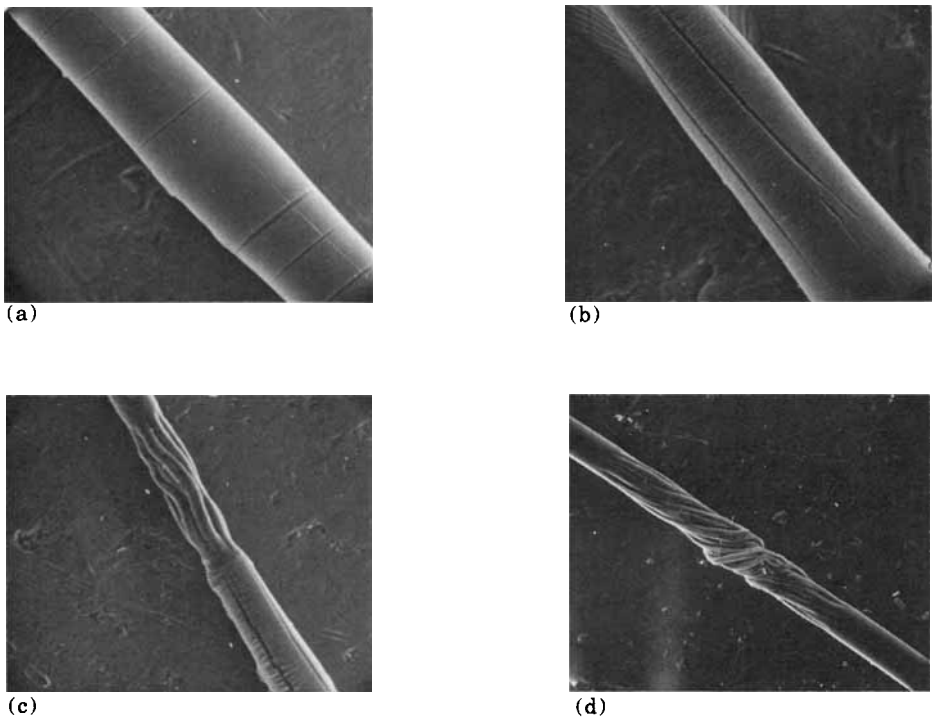

Fig. 2. Fracture morphology of 1.65 DR PET fibers showing crack initiation and propagation, nonimal tension 0.188 mN/dtex, strain amplitude 15°: (a) after 1000 cycles, 96×; (b) after 3000 cycles, 240×; (c) after 6000 cycles, 96×; (d) after 12,000 cycles, 96×.

torsional fatigue. The strength losses, thereafter, are less rapid than that of lower draw ratio fiber. The torsional fatigue life of the structure is extended by a factor of about 10 over that of 1.65 DR PET filaments. Longitudinal cracks appear at cycling levels at which strength losses are becoming significant. The fibrillar bundles appear at longer fatigue time, but they have smaller dimensions compared to the lower draw ratio filaments as shown in Figures 4(a)–(c). Presumably, the different DR filaments

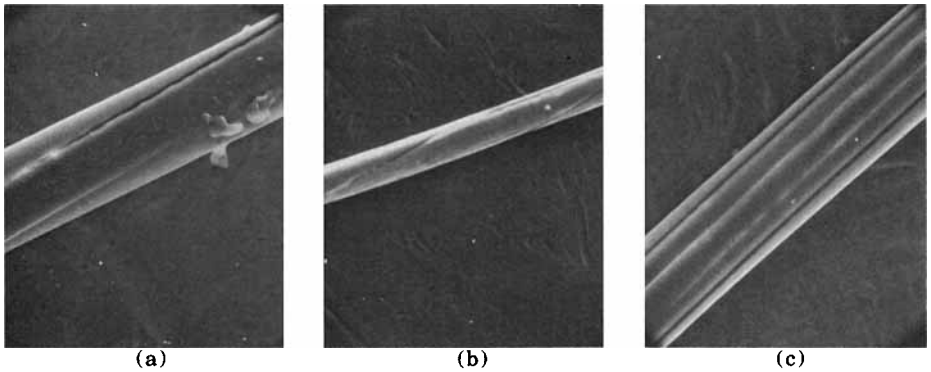

Fig. 3. Fracture morphology of torsionally fatigued 3.64 DR PET fibers showing crack initiation and propagation tension 0.188 mN/dtex, strain amplitude 15°: (a) after 3000 cycles, 225×; (b) after 6000 cycles, 90×; (c) after 15,000 cycles, 225×.

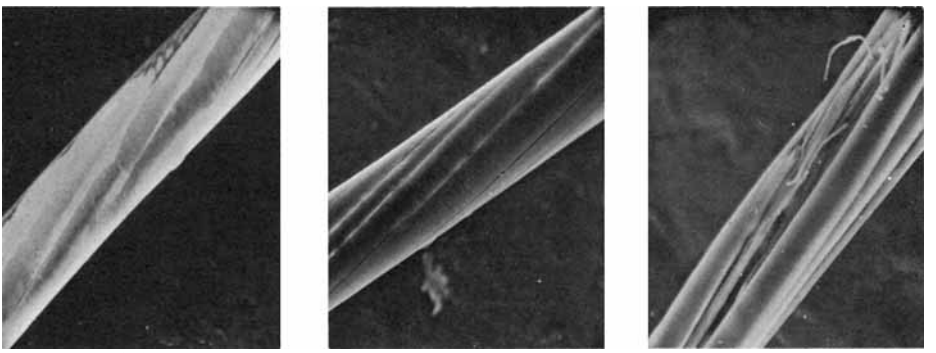

(a) (b) (c)

Fig. 4. Fracture morphology of torsionally fatigued 5.08 DR PET fibers showing crack initiation and propagation, tension 0.188 mN/dtex, strain amplitude, 15°: (a) after 3000 cycles, 225×; (b) after 12,000 cycles, 225×; (c) after 15,000 cycles, 225×.

behave differently because of their different fine structural features such as density, crystallinity, and orientation.

The effect of torsional amplitude on the fatigue behavior has also been examined, by altering the filament length undergoing torsional cycling. Torsional fatigue behavior was observed at three strain levels on the two fibers of lowest draw ratios (Figs. 5 and 6). The fatigue behavior was followed on the 5.08 DR filament at five levels of strain amplitude. (Fig. 7). As might be expected, a lowering of the strain amplitude increases the number of cycles required to reach different stages of torsional fatigue. In the case of the 1.65 DR filaments, the point of initial deterioration as observed through tensile strength losses is increased from 1000 cycles for $\alpha = 15°$ to more than 5000 cycles for $\alpha = 3°$. The overall pattern remains relatively the same afterwards, with the anomalous knee in the curve remaining near a relative strength of 0.4.

The region at which relative strength begins to drop is not too different for filaments having 3.64 DR. However, the lower anomalous knee is absent, and the strength losses are very uniform as the number of fatigue cycles are increased. In the case of torsional strain amplitudes of 7° and 15°, failure occurs following fatigue cycles that are more than twice those observed for the lowest draw ratios. The pattern for the smallest strain of 3° is starkly different. Although the initiation of strength losses begins after about 5000 cycles, the rate of tensile load reduction is significantly reduced thereafter. Complete torsional fatigue rupture is not complete at 500,000 cycles. In fact, strength loss after that period (more than a week of continuous cycling) is only about 50%.

The patterns are similar for specimens of the highest draw ratio (5.08). Differences arise mainly in strain amplitudes for which failure occurs in less than one million cycles. Large strain amplitudes of 11° and 15° are sufficient to completely eliminate any load carrying capacity prior to a million cycles (11 days of continuous cycling). All strain amplitudes of 7° or less only lowered the relative tensile strengths in proportion to the strain amplitudes. Again, high draw ratios lead to better torsional fatigue resistance.

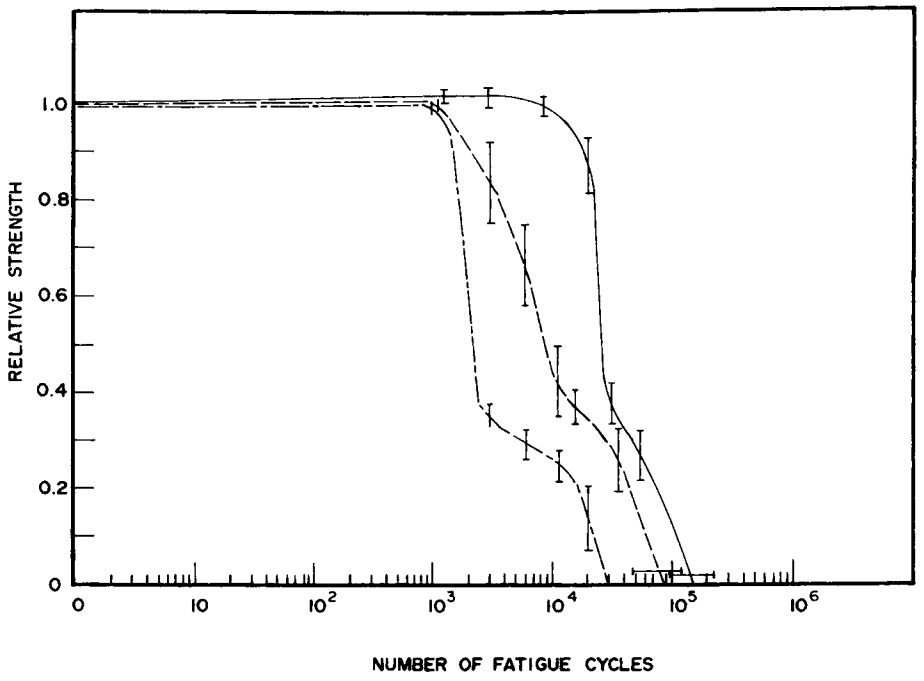

Fig. 5. Fatigue cycles vs. relative strength at various strain amplitudes for 1.65 DR PET fibers. α: (—) 3°; (- - -) 7°; (— · —) 15°.

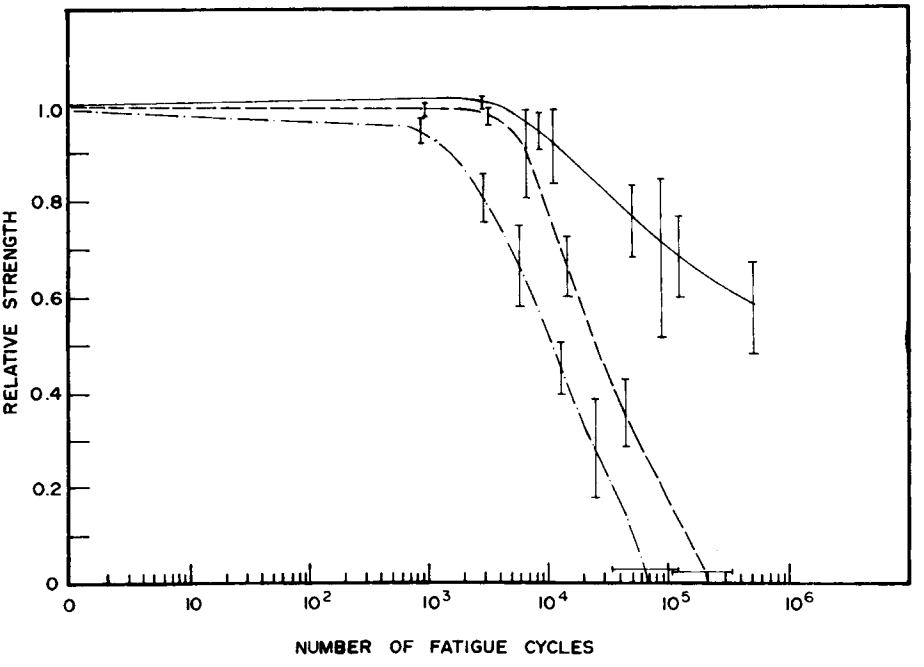

Fig. 6. Fatigue cycles vs. relative strength at various strain amplitudes for 3.64 DR PET fibers. α: (—) 3°; (- - -) 7°; (— · —) 15°.

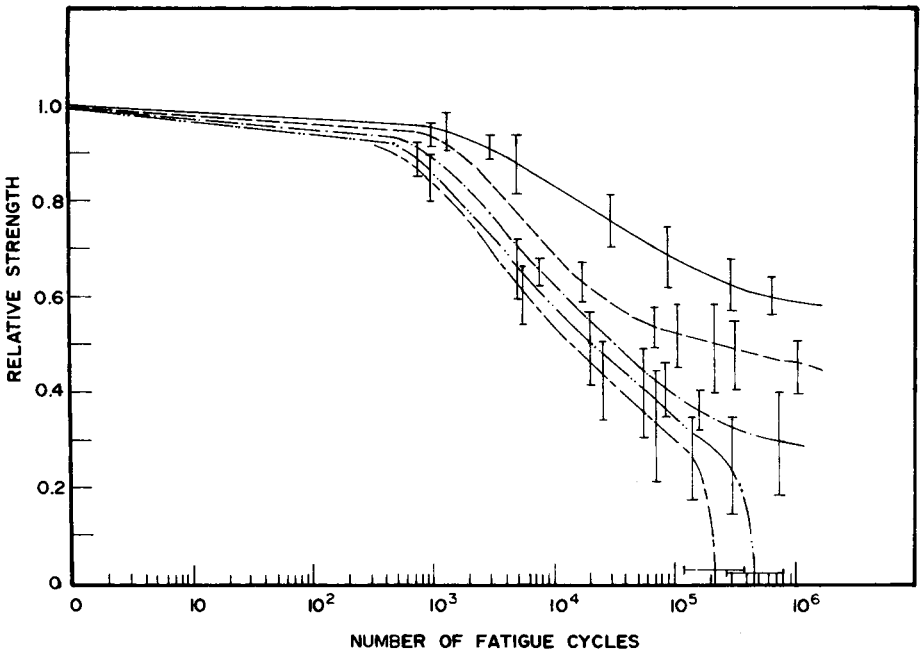

Fig. 7. Fatigue cycles vs. relative strength at various strain amplitudes for 5.08 DR PET fibers. α: (—) 3°; (- - -) 5°; (— • —) 7° (— • • —) 11°; (— - —) 15°.

Torsional Fatigue Mechanism

Peterlin[15] has formulated the development of morphology in drawn fibers and has thoroughly discussed the formation of microvoids and the disruption of lamellae. Sze, Spruiell, and White[16] have suggested a phenomenological explanation of the formation of voids in high density polyethylene and have conjectured that when a quasitransformation from a low modulus to high modulus phase occurs, the complex stress field around microvoids or defects near phase boundaries will cause them to enlarge into voids which are elongated in the direction of the stress field. This phenomenon results in fibrillation of the structure and the intensity of fibrillation will change with draw ratio. This type of phenomenon is also observed in melt spun-drawn polyester filaments as is evident from SEM photomicrographs of drawn peeled, twisted fibers (Fig. 8).

When a filament of radius r is twisted through an angle θ about its axis, this results in a strain $r\theta$ and a shear stress $Gr\theta$, where G is the shear modulus. The shear stress increases linearly with radius. The resulting torsional deformation can result in plastic yielding, and tension in the filament if axial contraction of the filament is prevented. This plastic yielding first occurs at the surface layers of the filament even at small torsional angle. As the fatigue process proceeds, the plastic yield point moves radially inwards, and the stress concentration at the crack front generates voids, which gradually enlarge due to microvoid coalesence. It has been suggested that the width of cracks in the direction normal to the tensile stress axis are relatively stable in a polymer and are determined by the structural

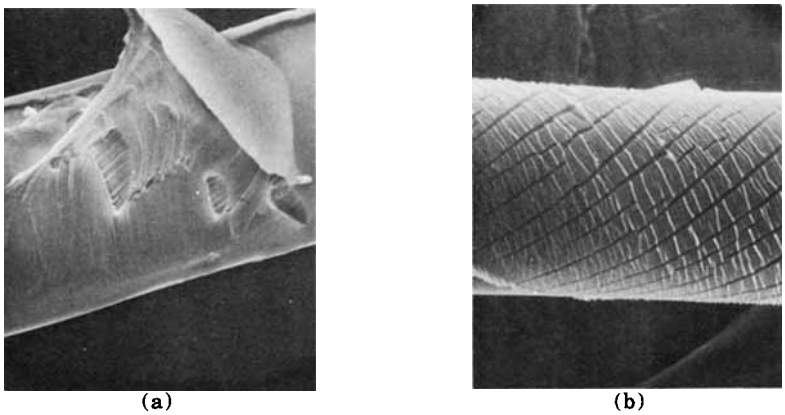

(a) (b)

Fig. 8. Fracture morphology of twisted 5.08 DR PET fibers: (a) twisted to 40 turns per cm, and peeled, 500×; (b) twisted to 55 turns per cm, 500×.

element sizes. The apparent depth of an individual crack as observed by examining the surface of the fiber seems to be a function of the density of cracks, which in turn is dependent upon crystallinity and draw ratio of the fiber.

During the drawing process and the subsequent mechanical deformation, microcracks and macrocracks are transformed into channels directed along the axis of tension. The repeated dynamic loading process intensifies the interaction between submicrocracks (cracks of sizes less than microscopic dimensions), and this subsequently decreases the effective cross section of the material sharing the load. The result is an increase in the mean stress on the active part of the cross section. This further enhances the coalescence and enlargement of cracks observed in the fracture morphology of fibers of various draw ratios. The number and size distribution of fibrils (and microfibrils) in the fractured surface are strongly influenced by the number and size distribution of submicrocracks. It is also evident from the SEM photomicrographs that the number and size distribution of fibrillar units formed at the fracture failure point are closely related to the draw ratio *vis à vis* orientation as shown in Figures 9(a)–(f).

Differences in fatigue fracture morphologies such as the initiation phenomenon, mechanical degradation, reduction in strength, and the number and size of fibrils formed after fatigue failure, due to variation in molecular orientation (via draw ratio) and crystallinity, may be graphically explained using the somewhat oversimplified models shown in Figures 10(a), (b), and (c).

At low draw ratios (1.65 DR) the internal structure of the fiber has little observable fibrillar structure [Fig. 11(a)]. The internal morphology shows a more or less homogeneous structure with low crystallinity. When the fiber is subjected to repeated cyclic torsional deformation, the fiber surface initially shows the development of cracks perpendicular to the fiber axis [Fig. 2(a)]. Further cyclic loading induces the onset of large scale intersegmental displacement, resulting in yielding of the structure in shear as well as in

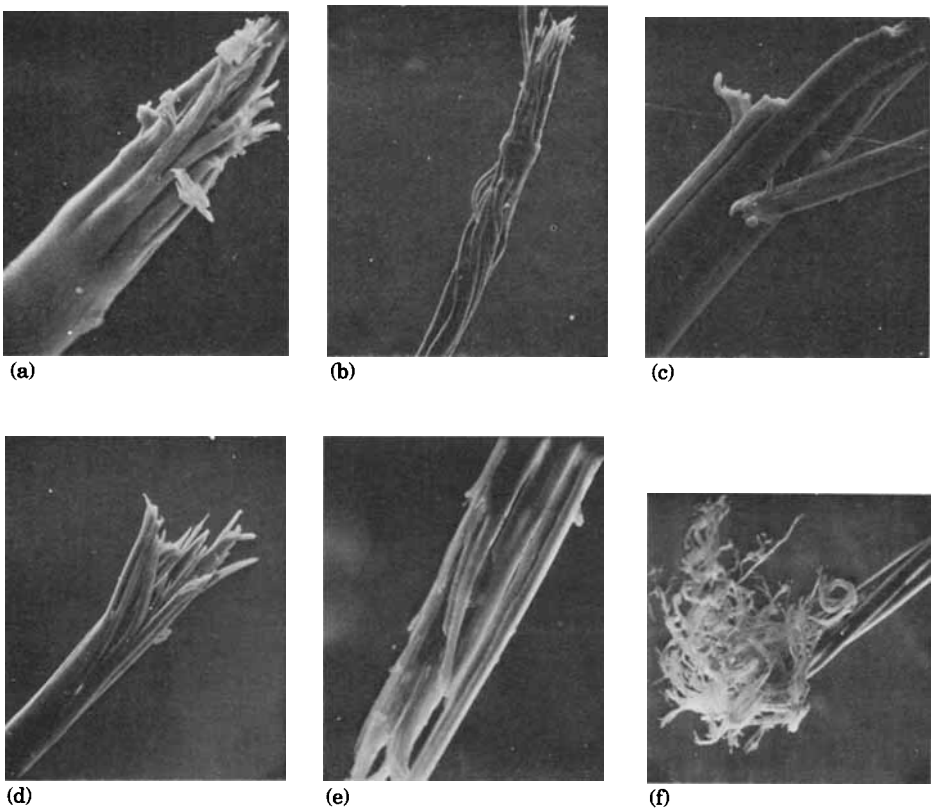

Fig. 9. Fractured ends of torsionally fatigued and broken in tensile tests PET fibers, tension 0.188 mN/dtex, strain amplitude 15°: (a) 1.65 DR—after 3000 cycles, 225×; (b) 1.65 DR—after 27,000 cycles 90×; (c) 3.64 DR—6000 cycles, 90×; (d) 3.64 DR—60,000 cycles, 90×; (e) 5.08 DR—21,000 cycles, 225×; (f) 5.08 DR—150,000 cycles, 90×.

tension. Early stages of fibrillation along the fiber axis occur while extended cycling produces drawing and necking of the structure [Fig. 2(a), (d)]. The degradation of the structure and the ropelike segmentation could perhaps be attributed to the onset of initial transverse cracks and nonuniformity in the stress distribution due to variation in filament diameter. The cracks will act as stress concentrators (in successive cycling) and would advance rapidly inwards to cause failure from shear yielding at these regions. This process is shown graphically in Figure 10(a).

With increasing draw ratio, the fiber internal structure exhibits heterogeneity in terms of fibrillar formation, as depicted in Figures 11(b) and (c). At medium draw ratio (3.64 DR) the outer layers show much higher molecular orientation which gradually decreases toward the center (core) of the fiber. On the other hand, the highly drawn fiber (5.08 DR) exhibits a highly developed fibrillar structure with the fibrillar bundles oriented along the fiber axis. The mechanism operating in this situation appears to be a breakdown of the material between the fibrils from stresses to cause slippage between fibrils in the initial stages of torsional fatigue process as

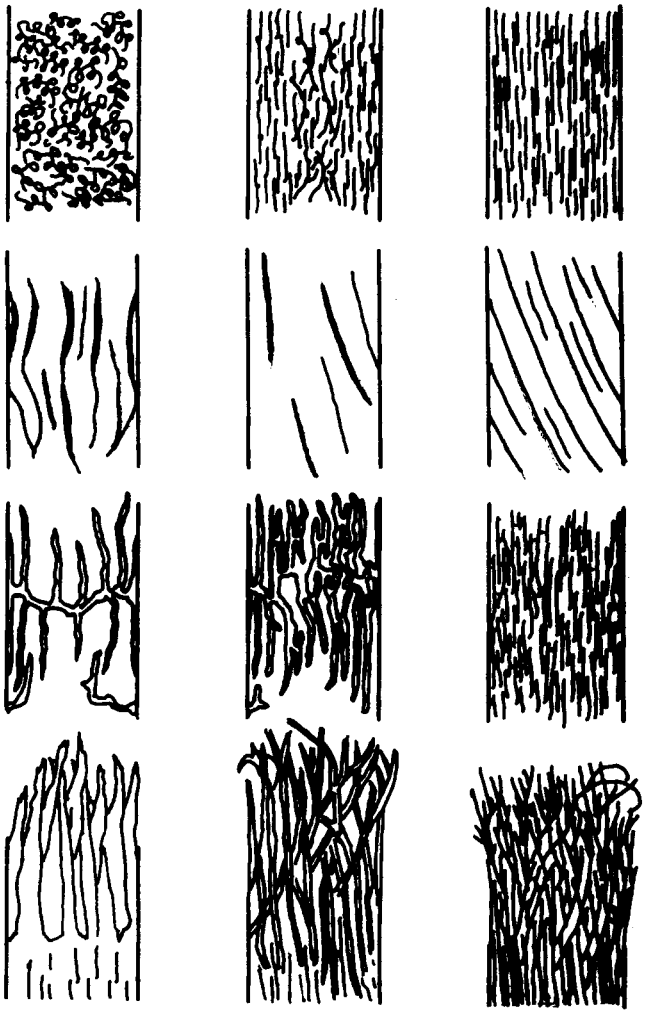

Fig. 10. Model showing the process of crack initiation, propagation and fracture of torsionally fatigued PET fibers: (a) low draw ratio; (b) medium draw ratio; (c) high draw ratio.

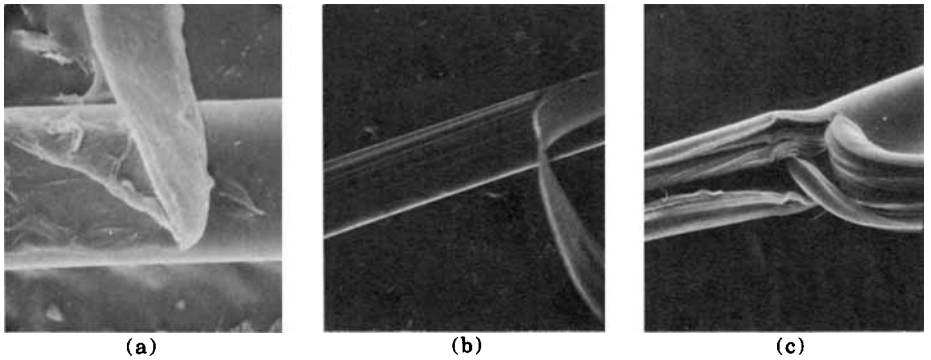

Fig. 11. Peeled PET fibers showing internal structure: (a) 1.65 DR, 450×; (b) 3.64 DR, 225×; (c) 5.08 DR, 225×.

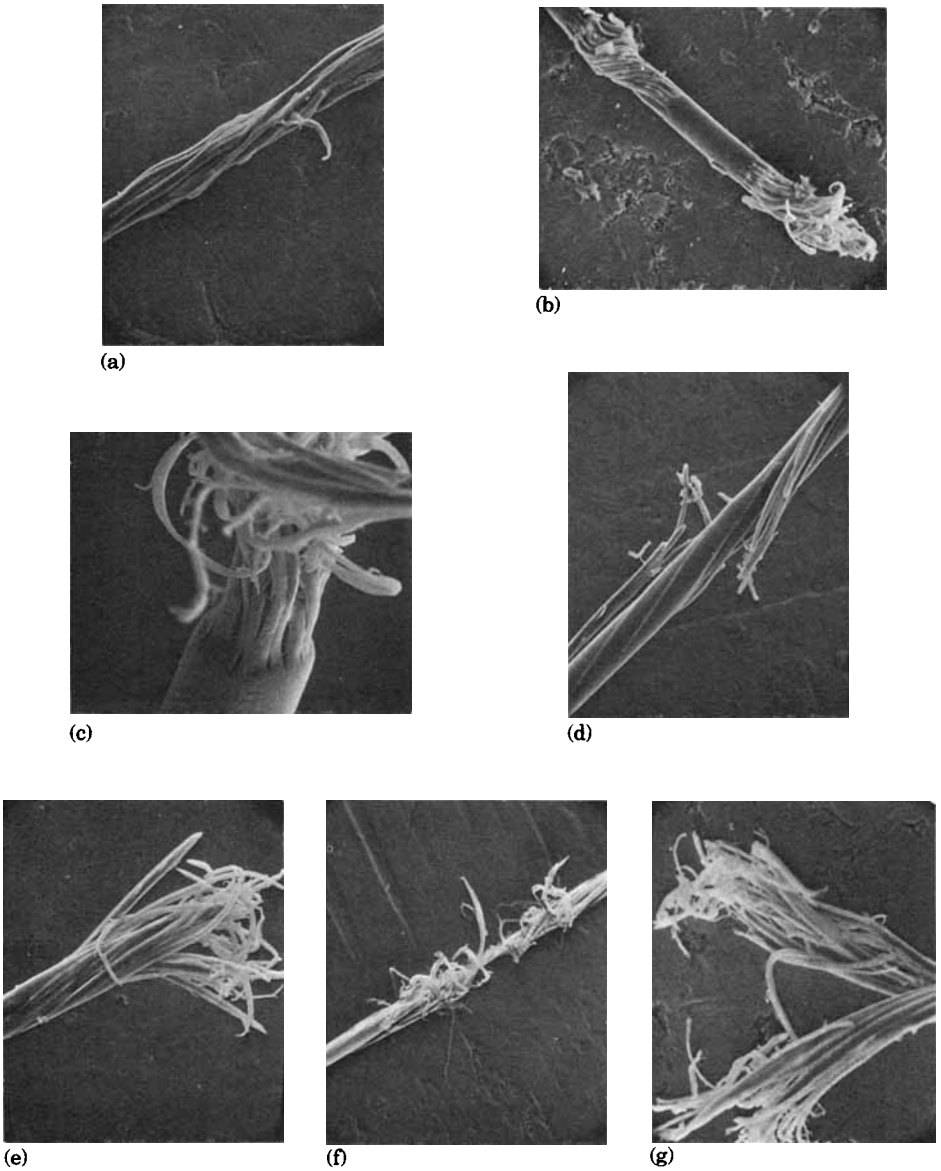

Fig. 12. Photomicrographs showing gradual rupture of fatigued PET fibers, tension 0.188 mN/dtex; strain amplitude 15°; (a) 1.64 DR after 27,000 cycles, 90×; (b) 1.64 DR ruptured after 36,000 cycles, 90×; and (c) 1.64 DR ruptured after 48,000 cycles, 225×; (d) 3.64 DR after 60,000 cycles, 90×; (e) 3.64 DR ruptured after 66,000 cycles, 90×; (f) 5.08 DR after 210,000 cycles 45×; (g) 5.08 DR ruptured after 306,000 cycles, 90×.

evidenced from the development of numerous longitudinal cracks along the fiber. During subsequent straining a large part of the strain energy is dissipated in further breakdown of the structure to microfibrils. The time required to rupture the structure is determined by the initial extent of fibrillar development in the structure. This is apparent from the intermediate and final fracture morphology of the fiber ends as apparent from

the severity of fibrillation as shown in Figures 12(a)–(g). The mechanism leading to fibrillation in medium and high draw ratio monofillaments is schematicaly depicted in Figure 10(b) and (c).

CONCLUSIONS

From the limited experimental data presented here, it is obvious that the fracture morphology and the residual strength after fatigue of poly(ethylene terephthalate) fibers is strongly affected by the torsional strain amplitude. There is some evidence of a critical strain amplitude beyond which the fiber shows rapid drop in strength. The number of cycles to rupture are highly dependent on the initial development of fibrillar structure. Highly drawn and crystalline fibers (heterogeneous structures) require an extremely large number of fatigue cycles to rupture relative to low oriented homogenous structures.

References

1. V. Bouda and A. J. Staverman, *J. Polym. Sci.*, Polym. Phys. Ed., **14**, 2313–2323 (1976).
2. W. J. Lyons, *Text. Res. J.*, **32**, 448 (1962).
3. W. J. Lyons, *Text. Res. J.*, **32**, 750 (1962).
4. J. W. S. Hearle, *J. Mater. Sci.*, **2**, 474 (1967).
5. J. W. S. Hearle and E. A. Vaughn, *Rheol. Acta*, **9**(1), (1970).
6. B. C. Goswami and J. W. S. Hearle, *Text. Res. J.*, **46**, 55 (1976).
7. A. R. Bunsell and J. W. S. Hearle, *J. Appl. Polym. Sci.*, **18**, 267–291 (1974).
8. A. K. Van der Vegt, *Rheol. Acta* **2**, 17 (1962).
9. B. C. Goswami, K. E. Duckett, and T. L. Vigo, *Text. Res. J.*, **50**, (1980).
10. K. E. Duckett and B. C. Goswami, *Text. Res. J.*, **54**, 43–46 (1984).
11. H. H. Kausch, *Polymer Fracture*, New York, 1978.
12. G. Farrow, *Polymer*, **1**, 518 (1960).
13. G. Farrow and D. Preston, *Br. J. Appl. Phys.*, **11**, 353 (1960).
14. J. H. Dumbleton, *J. Polym. Sci., A-2*, **6**,795 (1968).
15. A. Peterlin, *Int. J. Fracture*, **11**(5), 761–780 (1975).
16. Gordon M. Sze, J. E. Spruiell, and J. L. White, *J. Appl. Polym. Sci.*, **20**, 1823–1847 (1976).

Received June 6, 1984
Accepted August 31, 1984